


ORIGINAL ARTICLE

EIF3B stabilizes PTGS2 expression by counteracting MDM2-mediated ubiquitination to promote the development and progression of malignant melanoma

Pengli Fang¹ | Yikai Han¹ | Yanhong Qu² | Xin Wang³ | Yong Zhang⁴ | Wei Zhang⁵ | Na Zhang⁶ | Guangshuai Li⁷ | Wang Ma¹ 

¹Department of Oncology, The First Affiliated Hospital of Zhengzhou University, Zhengzhou, China

²Oncology Department of Laiyang People's Hospital, Laiyang, China

³Department of Radiotherapy, The First Affiliated Hospital of Zhengzhou University, Zhengzhou, China

⁴Department of Cancer Biotherapy Center, Affiliated Cancer Hospital of Zhengzhou University & Henan Cancer Hospital, Zhengzhou, China

⁵Department of Colorectal Surgery, The First Affiliated Hospital of Zhengzhou University, Zhengzhou, China

⁶Department of Dermatology, The First Affiliated Hospital of Zhengzhou University, Zhengzhou, China

⁷Department of Plastic Surgery, The First Affiliated Hospital of Zhengzhou University, Zhengzhou, China

Correspondence

Wang Ma, Department of Oncology, The First Affiliated Hospital of Zhengzhou University, No. 1 Jianshe Dong Road, Zhengzhou, Henan 450052, China.
Email: doctormawang@126.com

Guangshuai Li, Department of Plastic Surgery, The First Affiliated Hospital of Zhengzhou University, No. 1 Jianshe Dong Road, Zhengzhou, Henan 450052, China.
Email: liguangshuai@zzu.edu.cn

Funding information

Henan Physical Medicine Society Foundation, Grant/Award Number: 2021HYTP058

Abstract

Malignant melanoma (MM) is a neoplasm that develops from human melanocytes. It was reported that eukaryotic translation initiation factor 3 subunit B (EIF3B) is associated with multiple types of cancers, but its role in MM has not been reported. In the present study, we found that EIF3B was abundantly expressed in MM and was strongly related to lymphatic metastasis and pathological stage of MM patients. In addition, EIF3B depletion could block the progression of MM in vitro and in vivo. In contrast, EIF3B overexpression increased cell proliferation and migration in melanoma cells. More importantly, we identified that EIF3B's driver role in MM was mediated by PTGS2. In detail, we found that EIF3B stabilized PTGS2 expression by inhibiting PTGS2 ubiquitination, which is mediated by the E3 ligase MDM2. Moreover, like EIF3B, silencing PTGS2 could suppress MM development, and more interestingly, it could reverse the situation caused by overexpression of EIF3B in vitro and in vivo. Furthermore, the proliferation and migration inhibited by silencing of EIF3B were also partially recovered by overexpression of PTGS2. Overall, our findings revealed the potential of EIF3B as a therapeutic target for MM. Identification of EIF3B's function in MM may pave the way for future development of more specific and more effective targeted therapy strategies against MM.

KEYWORDS

EIF3B, malignant melanoma, PTGS2

Pengli Fang and Yikai Han contributed equally to this work.

This is an open access article under the terms of the [Creative Commons Attribution-NonCommercial-NoDerivs](https://creativecommons.org/licenses/by-nc-nd/4.0/) License, which permits use and distribution in any medium, provided the original work is properly cited, the use is non-commercial and no modifications or adaptations are made.

© 2022 The Authors. *Cancer Science* published by John Wiley & Sons Australia, Ltd on behalf of Japanese Cancer Association.

1 | INTRODUCTION

Malignant melanoma (MM) is a neoplasm that stems from human melanocytes.¹ MM mainly occurs in the skin, which is one of the most malignant and aggressive type of skin cancers.² According to the understanding of MM, the incidence of early metastasis is high, and the clinical prognosis for advanced patients is extremely poor.³ As such, early diagnosis and treatment are important for reducing morbidity and mortality. At the moment, the most commonly used method for MM patients is still surgical treatment, which could prolong the survival of patients to a certain degree.⁴ Nevertheless, in recent years, with the continuous deepening of MM research and the advancement of diagnosis and treatment technologies, target therapy has become a new prognosis improvement strategy for patients with MM.⁵⁻⁷ Thus, the objective in presenting this particular case is to explore the mechanism of MM pathogenesis so as to find out more potential therapeutic targets.

As is well known, translation is a key step in protein synthesis, and multiple translation initiation factors play important roles in this process.⁸ One of these factors is eukaryotic translation initiation factor (EIF), which is mainly responsible for the formation of the initiation complex.⁹ EIF3 is a central member of the EIF family. Given that it contains 13 different protein subunits (named EIF3A to EIF3M), EIF3 is considered the largest and most complex factor, and these subunits cooperatively participate in the entire process of translation initiation.¹⁰ What we focused on here is the EIF3B subunit, also called EIF3p110, EIF3p116, and hPrt1, which is widely regarded as a critical scaffold protein in the EIF3 complex and is involved in translation regulation and cell growth.^{10,11} Existing literature has reported that EIF3B is highly expressed in several types of cancers, such as clear cell renal cell carcinoma,¹² esophageal squamous cell carcinoma,¹³ gastric cancer,¹⁴ and bladder cancer,¹⁵ and high level of it leads to poor prognosis. However, little is known about the relevance of EIF3B in MM.

In the present study, we found that EIF3B was abundantly expressed in MM and was strongly related to lymphatic metastasis and pathological stage of MM patients. In addition, EIF3B depletion/elevation could curb/enhance the progression of MM. More importantly, we identified that the driver role played by EIF3B in MM was mediated by PTGS2. Like EIF3B, silencing PTGS2 could suppress MM development, and more interestingly, it could reverse the promotion effects caused by overexpression of EIF3B. Overall, our findings revealed the potential of EIF3B as a therapeutic target for MM.

2 | MATERIALS AND METHODS

2.1 | Tissue specimens and cell lines

Tissue microarrays, provided by Xi'an Alenabio Co., Ltd., yielded 164MM tissues and 26 normal tissues. All the patients signed informed consent before collecting samples. This study was approved

by the Laboratory Animal Center of Zhengzhou University [No. ZZU-LAC20200911 (18)].

Human epidermal melanocytes HEMa from the American Type Culture Collection (ATCC) and four human MM cell lines, including two invasive choroidal melanoma cells MUM-2C and MUM-2B from Cell Resource Center (Institute of Basic Medicine, Chinese Academy of Medical Sciences) and two MM cells A375 and SK-MEL-28 from BeNa Technology, were used in this study. The specific culture conditions for each cell type were as follows: Both invasive choroidal melanoma cells were grown in H-DMEM medium. A375 cells were cultured in DMEM, and SK-MEL-28 cells were cultured in 1640 medium. All media contained 10% FBS, and all the cells were placed in a 37°C incubator containing 5% CO₂. HEMa cells were cultivated using complete growth medium prepared according to the instructions of Adult Melanocyte Growth Kit (PCS-200-042™).

2.2 | Immunohistochemistry (IHC)

After soaking the tissue samples with xylene and washing with alcohol (China National Pharmaceutical Group Co., Ltd), the slides were repaired with 1×EDTA (Beyotime Biotechnology Co., Ltd) and blocked with 3% H₂O₂ and serum. After that, the slides were incubated with EIF3B, PTGS2, or Ki-67 antibodies and a subsequent second antibody at 4°C overnight and then stained with DAB and hematoxylin (Baso Diagnostics Inc.). Finally, the slides were sealed with neutral resin (China National Pharmaceutical Group Co., Ltd). Two pathologists independently and randomly examined all slides. Positive cells were scored as: 1 (1%-24%), 2 (25%-49%), 3 (50%-74%) and 4 (75%-100%), while staining intensity was scored from 0 (signal-less color) to 3 (light yellow, brown, and dark brown). IHC outcomes were determined as negative (0), positive (1-4), ++ positive (5-8), or +++ positive (9-12) with reference to positive cell score and staining intensity. Finally, we determined high- and moderate-expression parameters by taking the median of all IHC experimental scores of all tissues. Antibodies used in this section are listed in Table S1.

2.3 | Plasmid construction and lentivirus transfection

The corresponding EIF3B and PTGS2 RNAi target sequences, as well as EIF3B/PTGS2 overexpression sequences, were designed by Shanghai Bioscience Co., Ltd. and subsequently were inserted into the BR-V-108 vector through the restriction sites at both ends and transformed into TOP 10 *E. coli* competent cells (Tiangen). The plasmids of positive recombinants were extracted with the EndoFree maxi plasmid kit (Tiangen), and the concentration was determined in a spectrophotometer (Thermo_Nanodrop 2000).

For lentivirus transfection into MM cells, the cells in the logarithmic growth period were transfected by adding 20μl 1×10⁸ TU/ml lentivirus under the transfected condition of ENI.S+Polybrene and then were respectively cultured in DMEM and 1640 medium (both

containing 10% FBS) in a six-well dish (2×10^5 cells/well). Finally, the transfection efficiency of lentivirus and knockdown/overexpression efficiency of EIF3B and PTGS2 were evaluated by microscopic fluorescence, qRT-PCR, and Western blot.

2.4 | RNA extraction, cDNA synthesis, and qRT-PCR

Total RNA was isolated using TRIzol reagent (Sigma) from both MM cell lines, and then cDNA synthesis and qRT-PCR were performed using the Promega M-MLV kit (Promega Corporation) and the SYBR Green Master Mix kit (Vazyme). GAPDH was as an internal normalization control. The relative expression of mRNA was evaluated based on the $2^{-\Delta\Delta Ct}$ method. The primer sequences (5'-3') are listed in Table S2.

2.5 | Western blot assay and co-immunoprecipitation (co-IP)

Malignant melanoma (MM) cells were collected after transfecting lentivirus and were lysed with $1 \times$ lysis buffer (Cell Signal Technology) to harvest protein. Protein purity was quantified with BCA methods. After that, 10% SDS-PAGE was used to segregate total proteins and transferred into PVDF membranes. Next, the membranes were blocked in TBST solution with 5% nonfat milk, subsequently incubated with primary antibodies and secondary antibodies, and then washed with TBST solution three times (for 10 minutes each time). Finally, the ECL+plus™ Western blotting system kit was used for color rendering, and X-ray imaging was captured. For co-IP assay, proteins of A375 cells were collected and immunoprecipitated by anti-PTGS2, anti-MDM2, and IgG antibodies and then subjected to Western blotting with antibody to EIF3B, PTGS2, and MDM2. Antibodies used here are shown in Table S1.

2.6 | Cell proliferation detection

For MTT assay, both MM cells with downregulated EIF3B were collected, digested, and resuspended into the cell suspension. A total of $100 \mu\text{l}$ cell suspension was cultured in 96-well plates at a cell density of 2000 cells and determined for 5 days; $20 \mu\text{l}$ MTT (5 mg/ml) and $100 \mu\text{l}$ DMSO were added into the 96-well plates. Optical density (OD) value at 490 nm wave length was detected with microplate reader (Tecan infinite).

For Celigo cell-counting assay, MM cells with indicated lentiviruses were collected and seeded into 96-well plates at a density of 2000 cells/well, placing in an incubator with 5% CO_2 at 37°C . The cell images were taken by Celigo image cytometer (Nexcelom Bioscience), and a continuous 5-day cell proliferation curve was drawn.

2.7 | Colony formation assay

A375 cells, with overexpressed EIF3B, downregulated PTGS2, and overexpressed EIF3B plus downregulated PTGS2 were harvested, digested, and seeded into a six-well plate (2 ml/well) for 5 days to form colony. Visible clones in the six-well plate were recorded by fluorescence microscope (Olympus). Finally, the cells were washed with PBS, fixed with 1 ml 4% paraformaldehyde, and stained by $500 \mu\text{l}$ Giemsa (Dingguo) to calculate the number of colonies.

2.8 | Cell migration assay

One method used for cell migration detection was transwell assay. MM cells with indicated lentiviruses were cultured to adjust the density of cells as 1×10^5 cells/ml. Subsequently, cells were loaded into the upper chamber containing serum-free medium. Then, the upper chamber was transferred to the lower chamber with 30% FBS and incubated for 72 hours. Finally, $400 \mu\text{l}$ Giemsa was used for cell staining, and the cell migration ability was quantified.

Another method was wound-healing assay. MM cells with indicated lentiviruses were seeded into a 96-well plate (5×10^4 cells/well). Then, the cells were incubated in an incubator with 5% CO_2 at 37°C and observed in a microscope at 8 and 24 hours. The experiment was repeated three times, and the migration rate of cells was evaluated based on the scratch images.

2.9 | Flow cytometry assay

For cell apoptosis, lentivirus-transfected A375 and SK-MEL-28 cells were cultured in six-well plates (2 ml/well) for 5 days. A total of $10 \mu\text{l}$ annexin V-APC was added for 10-15 minutes at room temperature in the dark for staining. The cell apoptosis level was measured by using FACSCalibur (BD Biosciences).

The lentivirus-transfected A375 and SK-MEL-28 cells were cultured in 6-cm dishes (5 ml/well) for cell cycle detection. The cells were stained for 30 minutes using cell-staining solution. The percentage of the cells in different phases was compared. Each experiment was repeated three times.

2.10 | Human apoptosis antibody array

The effects of depletion of EIF3B on the apoptosis-related protein expression in A375 cells were detected by the human apoptosis antibody array. After the cells were lysed, the handling array membranes were blocked in $2 \text{ ml } 1 \times$ Wash Buffer II and incubated with cell lysates and $1 \times$ biotin-conjugated anti-cytokines overnight at 4°C . Finally, the signals of membranes were tracked by chemiluminescence imaging system.

2.11 | PrimeView human gene expression array

Total RNA was extracted as described previously. The quality and integrity of RNA were determined by Nanodrop 2000 (Thermo Fisher Scientific) and Agilent 2100 and Agilent RNA 6000 Nano kit (Agilent). Referring to the manufacturer's instruction, cDNA array analysis was performed with Affymetrix human GeneChip PrimeView, and the data were scanned by Affymetrix Scanner 3000 (Affymetrix). The statistical significance of raw data was completed by using a Welch *t* test with Benjamini-Hochberg FDR ($|\text{Fold Change}| \geq 1.3$ and $\text{FDR} < 0.05$ as significant). Significant difference analysis and functional analysis based on ingenuity pathway analysis (IPA) (Qiagen) was executed, and $|Z\text{-score}| > 0$ was considered significant.

2.12 | The construction of a nude mouse tumor formation model

All animal experiments conformed to the European Parliament Directive (2010/63/EU) and were approved by the Laboratory Animal Center of Zhengzhou University [No. ZZU-LAC20200911 (18)].

Four-week-old female BALB-c nude mice (Shanghai Lingchang Animal Research Co., Ltd.) were used to establish a xenograft model. The mice were randomly divided into the indicated groups ($n = 10$ /each group), and 4×10^6 A375 cells with indicated lentiviruses, respectively, were suspended in $100 \mu\text{l}$ of PBS and subcutaneously injected subcutaneously into nude mice. The tumor volume was tested during the entire feeding period. On the last day of feeding, 0.7% sodium pentobarbital was injected intraperitoneally for several minutes, and the fluorescence was observed by the in vivo imaging

system (IVIS Spectrum, Perkin Elmer). After 14 days, the mice were sacrificed, and the tumors were removed to be weighed and photographed and were finally frozen in liquid nitrogen and stored at -80°C .

2.13 | Analyses of protein degradation

To analyze protein degradation at 24 hours after infection, A375 and SK-MEL-28 cells were treated with 0.2 mg/ml cycloheximide (CHX) and harvested at various time points. The cell lysates were subjected to immunoblotting. To analyze the protein ubiquitination of PTGS2, cells were cotransfected with PTGS2 and ubiquitin. At 24 hours after infection, the proteasome inhibitor MG132 ($10 \mu\text{M}$) was added, and the cells were incubated for 6 hours. PTGS2 antibody was added to the cell lysates and incubated overnight at 4°C . Protein A/G Plus-agarose was added, and the mixture was incubated for 4 hours at 4°C . Ubiquitin was detected using ubiquitin antibody. The antibodies used are listed in Table S1.

2.14 | Statistical analysis

Statistical analysis was carried out using GraphPad Prism 8 and SPSS 19.0 (IBM, SPSS). All data were presented as the mean \pm SD from at least three repeated experiments. Student's *t* test (for comparisons of two groups) and one-way ANOVA (for multiple group comparisons) were used to analyze the statistical significance. The Spearman correlation analysis and Mann-Whitney *U* analysis were used to assess the association between EIF3B expression and pathological characteristics of MM patients. $p < 0.05$ was considered to be significantly different. All experiments were performed in triplicate.

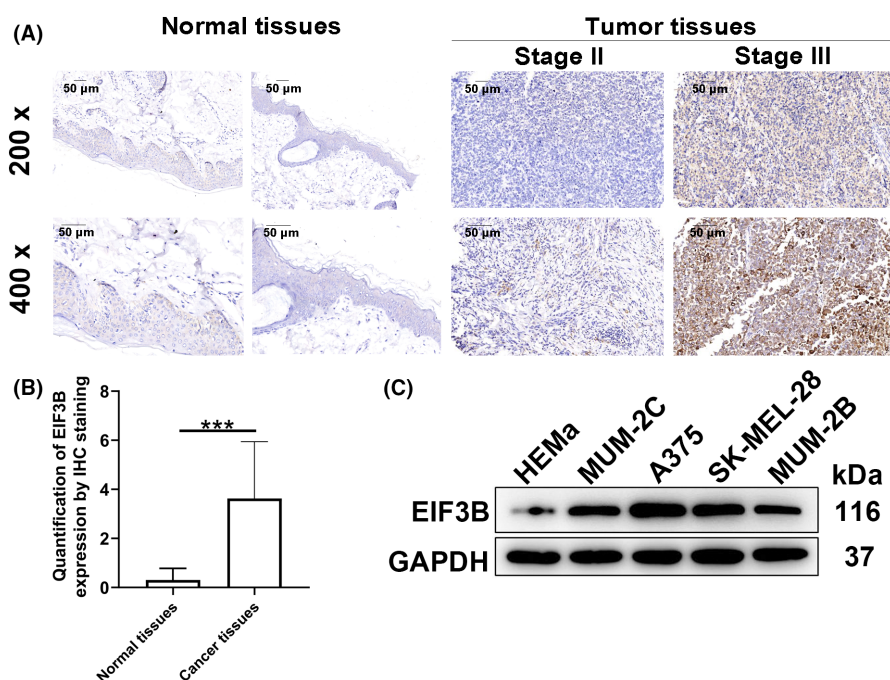


FIGURE 1 EIF3B was strongly expressed in malignant melanoma tissues and cells. A, B, The protein levels of EIF3B in 164 cases of malignant melanoma tumor tissues and 26 cases of paracarcinoma tissues were determined by immunohistochemical staining. C, The protein levels of EIF3B in human epidermal melanocytes HEMa and four malignant melanoma cells were detected by Western blotting. The experiment was performed in triplicate. Results are presented as mean \pm SD

3 | RESULTS

3.1 | EIF3B is elevated in MM and is associated with lymphatic metastasis and pathological stage of patients

To determine whether EIF3B is strongly expressed in MM, we first detected EIF3B expression in MM and paracarcinoma tissues. The rate of EIF3B high expression in MM tissues was 54.3% (89/164), whereas that of EIF3B low expression in normal tissues was 100% (26/26) (Figure 1A,B and Table S3, $p < 0.001$). To further investigate the functional significance of EIF3B expression in the development and progression of MM, we evaluated the relationship between EIF3B levels with clinicopathological characteristics provided by 89 melanoma patients. We obtained significant correlations between EIF3B expression with lymphatic metastasis and pathological stage (Table 1, $p < 0.01$ for lymphatic metastasis; $p < 0.05$ for pathological stage). Consistently, the Spearman's rank correlation analysis again confirmed that EIF3B expression correlated with lymphatic metastasis and pathological stage (Table S4). In addition, we detected EIF3B protein levels in human epidermal melanocytes HEMa and a panel of MM cells A375, SK-MEL-28, MUM-2C, and MUM-2B, showing that EIF3B was highly expressed in MM cells compared with HEMa cells (Figure 1C). On this account, EIF3B might be a potential driver for MM progression.

3.2 | EIF3B depletion/overexpression suppressed/enhanced proliferation and migration of melanoma tumor cells, blocked cell cycle, as well as enhanced cell apoptosis in vitro

To explore the role of EIF3B in MM pathogenesis, we assessed the effects of silencing EIF3B on tumor cell phenotypes. The successful knockdown of EIF3B in A375 and SK-MEL-28 cells was verified by observing intracellular fluorescence expression and detecting EIF3B mRNA and protein expression (Figure S1A–C). We then detected cell proliferation and migration capabilities after silencing EIF3B. Not surprisingly, obvious suppression was found in both cell proliferation and migration when EIF3B was downregulated (Figure 2A,B, $p < 0.001$). We also evaluated the expression levels of several EMT-related proteins, indicating downregulated N-cadherin, vimentin, and Snail, as presented in Figure 2C. In addition, EIF3B downregulation caused a decrease of cell percentage in S phase, as well as an increase of that in G2 phase (Figure 2D). Furthermore, EIF3B depletion accelerated cell apoptosis (Figure 2E, $p < 0.001$), via upregulating BIM, FasL, IGFBP-3, IGFBP-5, and TNF- β , combined with downregulating CD40, HSP60, HSP70, IGF-II, survivin, sTNF-R1, and XIAP (Figure 2F). Subsequently, Western blot assay revealed that P-Akt, CDK6 and PIK3CA were downregulated, while MAPK9 was upregulated upon silencing EIF3B (Figure 2G). To further confirm the effects of EIF3B in melanoma cells, EIF3B was overexpressed in A375 and MUM-2B cells. The results revealed that EIF3B overexpression

TABLE 1 Relationship between EIF3B expression and tumor characteristics in patients with malignant melanoma

Features	No. of patients	EIF3B expression		P value
		Low	High	
All patients	164	75	89	
Age (years)				
≤55	83	37	46	0.765
>55	81	38	43	
Gender	164			
Male	88	37	51	0.309
Female	76	38	38	
Tumor infiltrate				
T2	6	3	3	0.445
T3	26	7	19	
T4	71	29	42	
Lymphatic metastasis (N)				
N0	91	39	52	0.002
N1	10	0	10	
N2	4	0	4	
Stage				
I	6	3	3	0.040
II	81	34	47	
III	12	0	12	
IV	4	2	2	

significantly enhanced melanoma cell proliferation and migration (Figure S2A,B). These results suggested that EIF3B knockdown suppressed cell viability and migration in melanoma cells. In contrast, EIF3B overexpression increased cell proliferation and migration in melanoma cells.

3.3 | EIF3B facilitated melanoma tumor growth in vivo

Our in vitro studies have demonstrated that EIF3B enhanced melanoma cell malignant phenotypes. Therefore, we aimed to determine whether EIF3B is crucial for melanoma tumor growth in vivo. Melanoma animal models were established in 4-week-old male nude mice by subcutaneous injection of EIF3B-knockdown A375 cells (Figure 3A). As shown in Figure 3B, downregulation of the fluorescence intensity in the shEIF3B group indicated remarkable suppression of tumor growth ($p < 0.001$). In addition, further detection for characterization of tumors, including volume and weight, revealed a possible contribution of EIF3B depletion in impairing tumorigenesis ($p < 0.001$, Figure 3C–E). Fourteen days after cell injection, mice were sacrificed, and their tissues were separated for IHC analysis. As expected, tumor tissues from mice in the EIF3B-knockdown group showed dramatically downregulated Ki-67 (Figure 3F).

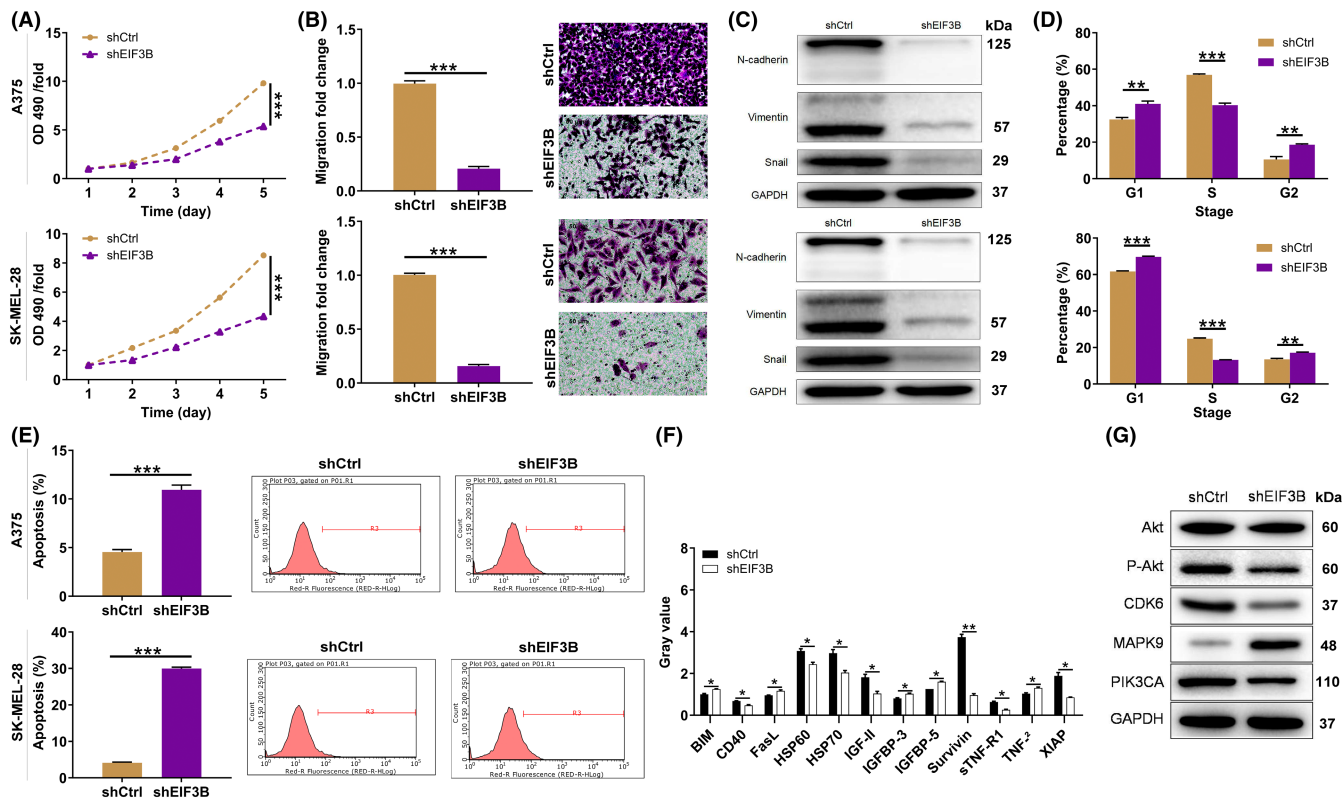


FIGURE 2 EIF3B knockdown/overexpression inhibited/enhanced malignant melanoma development in vitro. A, The cell proliferation rate was evaluated in A375 and SK-MEL-28 cells after transfecting shEIF3B by MTT assay. B, After transfecting shEIF3B, the migration rate of A375 and SK-MEL-28 cells was detected by transwell assay. Magnification: 200x. C, Western blot was used for detecting the levels of EMT-related proteins in A375 and SK-MEL-28 cells with downregulated EIF3B. D, E, The effects of EIF3B knockdown on cell cycle (D) and apoptosis (E) of A375 and SK-MEL-28 cells were examined by flow cytometry. F, The levels of apoptosis-related proteins in A375 cells transfected with shEIF3B were measured by ECL with human apoptosis antibody array. G, The expression of Akt, P-Akt, CDK6, MAPK9, and PIK3CA was detected by Western blot. All the experiments were performed in triplicate. Results are presented as mean \pm SD. * $p < 0.05$, ** $p < 0.01$, *** $p < 0.001$

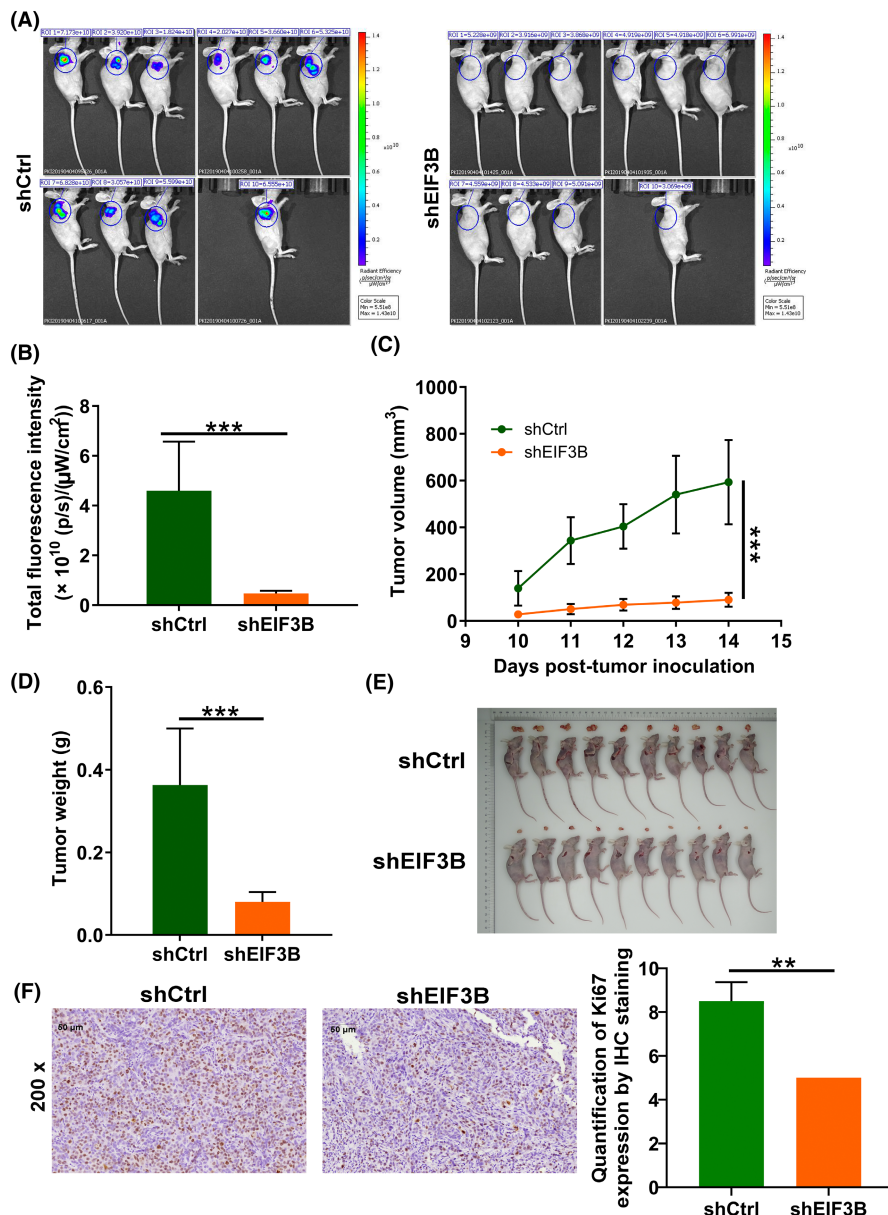
3.4 | PTGS2 is identified as the target gene of EIF3B regulating MM

To elucidate the underlying mechanism of EIF3B-mediated regulation of melanoma, we further employed a microarray analysis based on A375 cells, in which EIF3B was knock down, to investigate differentially expressed genes (DEGs). Taking fold change ≥ 1.3 and FDR < 0.05 as a reference, we obtained 488 upregulated and 559 downregulated genes in the shEIF3B group (Figure 4A). Given the canonical pathways analysis of IPA, we found that Superpathway of Cholesterol Biosynthesis, Cholesterol Biosynthesis, and ILK signaling were significantly suppressed (Figure 4B). Besides, we built up a network analysis between EIF3B and the above several pathways, indicating that EIF3B could affect HEX1M1, ACACA, NF2, FN1, HSD17B7, FDPS, HMGCR, IDI1, FDFT1, SQLE, SDC1, HMGCS1, MVD, TNF, CFL1, ITGB8, PIK3R2, PPARG, and PTGS2 in these pathways (Figure 4C). Next, we picked 19 significantly downregulated genes with relatively high fold changes for qPCR verification, among which four were subjected to Western blot assay, and found that PTGS2 was remarkably downregulated at both mRNA and protein levels (Figure 4D,E). Additional IHC analysis indicated that like EIF3B, PTGS2 was strongly expressed in

melanoma tissues relative to normal tissues (Figure S3A). Moreover, PTGS2 protein level was also abundant in MM cell lines relative to normal cells (Figure S3B). From the above, we proposed that PTGS2 might be a downstream target of EIF3B.

Here, one important question that remains is how EIF3B loss mechanistically affects PCNA expression. To solve this problem, we made preliminary explorations of molecular mechanisms. Unexpectedly, co-IP analysis suggested that there was a protein interaction between EIF3B and PTGS2 (Figure 4F). It is well known that protein modification plays an important role in cellular processes. Protein modification includes ubiquitination, methylation, acetylation, glycosylation, and phosphorylation.¹⁶ Herein, we first examined the protein stability of PTGS2 in CHX (a protein synthesis inhibitor)-treated A375 and SK-MEL-28 cells in which EIF3B was silenced and found that the degradation of PTGS2 protein was significantly accelerated by EIF3B knockdown (Figure 4G). Furthermore, after treatment with the proteasome inhibitor MG-132, the effects of EIF3B knockdown on the degradation of PTGS2 protein were partially abolished (Figure 4H), which implied that EIF3B may regulate PTGS2 through the ubiquitin-proteasome system (UPS). As is known, ubiquitination of proteins is usually involved in proteasome-mediated

FIGURE 3 EIF3B knockdown inhibited malignant melanoma tumor growth in vivo. **A**, A mice model was constructed via subcutaneous injection of shCtrl or shEIF3B A375 cells ($n = 10$ /each group). **B**, The fluorescence intensity in shCtrl and shEIF3B groups was obtained through injecting D-luciferase. **C**, The volume of tumors was checked from feeding to sacrifice. **D, E**, After sacrificing mice, the obtained tumors were weighed (**D**) and photographed (**E**). **F**, The value of Ki-67 was detected by immunohistochemistry (IHC) analysis in tumor sections from mice. Magnification: 200 \times . Results are presented as mean \pm SD. *** $p < 0.001$



degradation,^{17,18} so ubiquitination level of PTGS2 was further evaluated. As visualized in Figure 4I, EIF3B knockdown significantly augmented the ubiquitination of PTGS2. As EIF3B is not an E3 ligase, we further wondered how EIF3B affects the ubiquitination of PTGS2. By analyzing the Ubibrowser website (<http://ubibrowser.bio-it.cn/ubibrowser/strict/networkview/networkview/name/P35354/jobld/ubibrowse> I2022-07-22-74541-1658474603), we predicted that MDM2 was the ubiquitin E3 ligase that targets PTGS2. We thus hypothesized that MDM2 might be involved in the inhibition of the ubiquitin-mediated degradation of PTGS2 by EIF3B. The subsequent half-life analysis suggested that PTGS2 was much more unstable in MDM2-rich A375 and SK-MEL-28 cells (Figure 4J). More importantly, the ubiquitination of PTGS2 was improved in MDM2-rich cells (Figure 4K). We further validated the interaction of PTGS2 and MDM2 via co-IP (Figure 4L). Here, it was demonstrated that PTGS2 was the downstream target through which EIF3B participated in the regulation of MM.

3.5 | The promotion effects of EIF3B overexpression on melanoma progression were reversed via downregulating PTGS2

In order to investigate the effects of the EIF3B-PTGS2 axis in melanoma cells, we constructed merely overexpressing EIF3B and merely silencing PTGS2, as well as simultaneously overexpressing EIF3B and silencing PTGS2 lentiviral vectors to transfect A375 cells. Figure S4 definitely displays that the above three cell models were constructed well, so they were used in subsequent cell behavior experiments. The data of Celigo cell-counting assay showed that after lentivirus transfection, compared with the control group, A375 cells exhibited a higher proliferation rate ($p < 0.05$, fold change = 1.1) in the EIF3B group while a lower proliferation rate ($p < 0.001$, fold change = -3.9) in the shPTGS2 group. The promoted cell proliferation by overexpressing EIF3B could be rescued by silencing PTGS2 (Figure 5A). Moreover, the same phenomenon has also been observed in colony

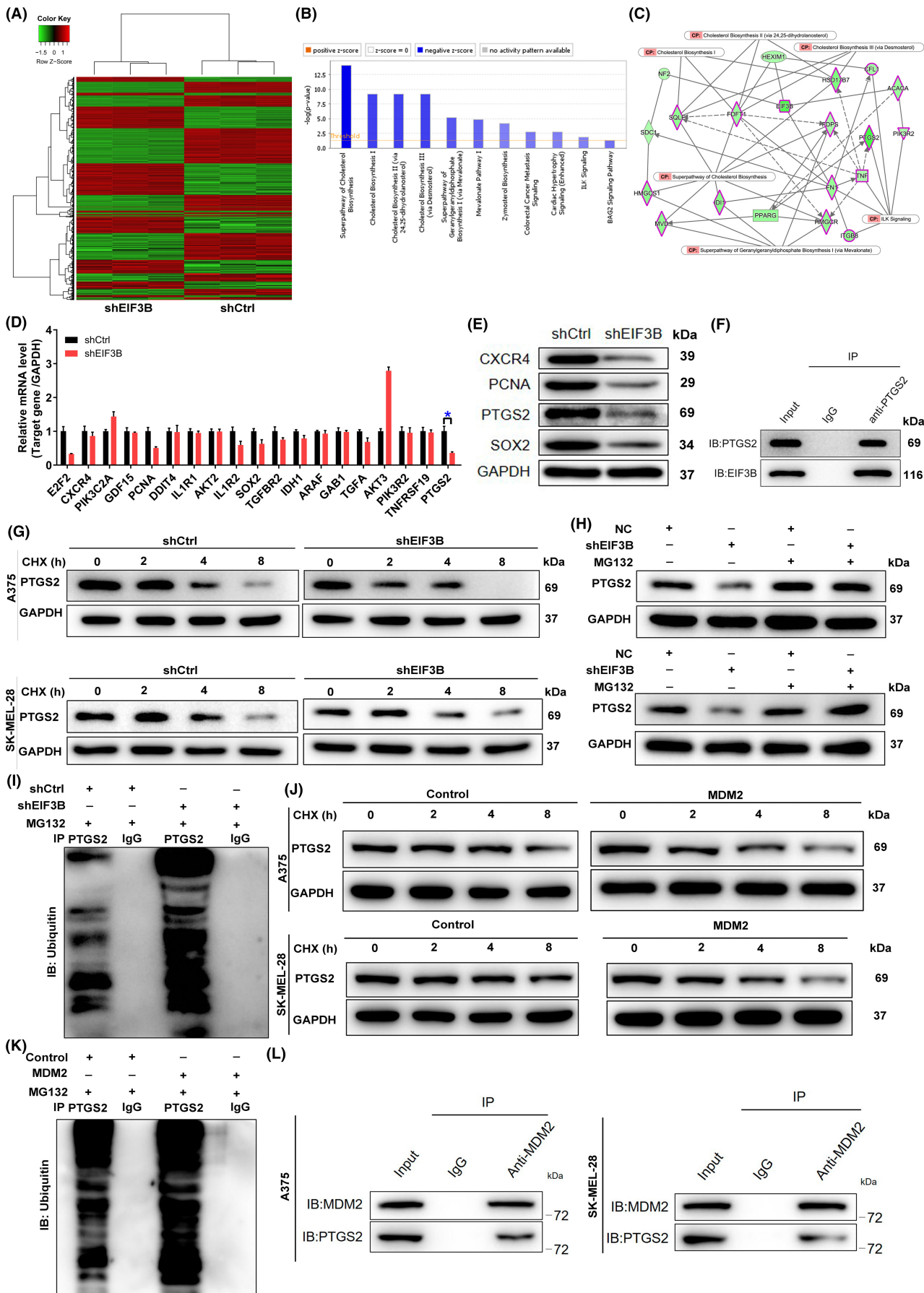


FIGURE 4 Exploration and verification of the underlying mechanism of EIF3B regulating malignant melanoma. A, Heatmap of differentially expressed genes (DEGs) identified by RNA sequencing of A375 cells treated with shCtrl ($n = 3$) or shEIF3B ($n = 3$). B, The enrichment of the DEGs in canonical signaling pathways was analyzed by ingenuity pathway analysis (IPA). C, Interaction network diagram between DEGs was analyzed by IPA. D, E, The expression of several of the most significant DEGs identified by qRT-PCR (D) and Western blot (E) in A375 cells with shEIF3B. The experiments were performed in triplicate. F, Co-immunoprecipitation (co-IP) assay was used to verify whether there was protein interaction between EIF3B and PTGS2. G, The protein levels of PTGS2 in EIF3B-depleted A375 and SK-MEL-28 cells were measured after 0.2 mg/ml CHX treatment for the indicated times. H, After treatment with MG-132, the protein levels of PTGS2 in EIF3B-depleted A375 and SK-MEL-28 cells were measured. I, The lysates of EIF3B-depleted A375 cells were subjected to immunoprecipitation, and Western blotting (WB) was performed to examine the ubiquitination of PTGS2. J, The protein levels of PTGS2 in MSM2-rich A375 and SK-MEL-28 cells were measured after 0.2 mg/ml CHX treatment for the indicated times. K, The lysates of MDM2-rich A375 cells were subjected to immunoprecipitation, and WB was performed to examine the ubiquitination of PTGS2. L, co-IP analysis of the interaction between PTGS2 and MDM2 in A375 and SK-MEL-28 cells. The data are expressed as the mean \pm SD ($n \geq 3$), * $p < 0.05$, ** $p < 0.01$, *** $p < 0.001$

formation and cell migration experiments (Figure 5B–D). As far as cell apoptosis is concerned, a trend to decreased cell apoptosis was found after EIF3B elevation ($p < 0.001$), which was also countermanded by inhibiting PTGS2 expression ($p < 0.001$, Figure 5E). On the other hand, we also evaluated the effects of the EIF3B-PTGS2 axis in another melanoma cell MUM-2B. Consistent with the data in A375 cells, overexpressing EIF3B also ameliorated MUM-2B cell proliferation and migration, which was partially abolished through knocking down PTGS2 (Figure 5SA–D). Furthermore, we constructed merely silencing EIF3B and merely overexpressing PTGS2, as well as simultaneously silencing EIF3B and overexpressing PTGS2 lentiviral vectors to transfect A375 cells. The observation for cell phenotypes showed that the proliferation and migration inhibited by silencing of EIF3B were partially recovered by overexpression of PTGS2 (Figure 5SE,F).

In order to address, whether this in vitro capacity results in a similar phenotype of tumor cells in vivo, we implanted A375 cells with indicated lentiviral vectors subcutaneously into immune-deficient mice and monitored tumor growth. As expected, the primary tumors derived from PTGS2-deficient cells grew slowly. In contrast, EIF3B-forced expression favored the growth of xenografts in nude mice, which was curbed through depleting PTGS2 (Figure 6A–E). Collectively, these data evidenced the effects of the EIF3B-PTGS2 axis in melanoma cells both in vitro and in vivo.

4 | DISCUSSION

With current treatment strategies, advanced melanoma is difficult to fight clinically¹⁹; therefore, the development of more novel and effective agents is particularly important for melanoma patients. According to reports, EIF3B is abnormally expressed or activated in multiple types of human cancers. For instance, EIF3B aggravates glioblastoma progression via promoting cell proliferation and inhibiting apoptosis.²⁰ In addition, it was reported that EIF3B expression is closely associated with the prognosis of human bladder cancer,¹⁵ esophageal squamous cell carcinoma,¹³ and prostate cancer²¹ and is required for tumor growth. However, the significance of EIF3B in MM is not quite clear.

Hence, our study first investigated the functional roles of EIF3B in the development and progression of MM. We found that EIF3B was abundantly expressed in both MM tissues and cell lines, which is statistically significant and correlated with lymphatic metastasis and pathological stage. Moreover, we used short-hairpin RNA to silence EIF3B in both MM cell lines with higher EIF3B levels and found that downregulation of EIF3B played a tumor-suppressing role in vitro via blocking cell proliferation, migration, and enhancing cell apoptosis. This was also verified by additional in vivo data. Then, we examined how EIF3B regulates the progress of MM. We found that upon silencing EIF3B, PTGS2 mRNA and protein levels were markedly decreased. The protein interaction of PTGS2 with EIF3B was also further validated. We further explored the specific regulatory mechanism between EIF3B and PTGS2 in mediating MM. The UPS plays an important role in cellular processes for protein quality control and homeostasis.²² Dysregulation of the UPS has been implicated in numerous diseases, including cancer. Indeed, components of the UPS are frequently mutated or abnormally expressed in various cancers.^{23,24} In this study, we found that EIF3B could affect the E3 ligase MDM2-mediated ubiquitination of PTGS2.

PTGS2 (aka COX-2) is one of two isoforms of prostaglandin endoperoxide synthase (also referred to as COX). COX, produced by damaged cell membranes, is mainly involved in the conversion of arachidonic acid into prostaglandins as a kind of rate-limiting enzyme. Unlike another isoform PTGS1 (COX-1), PTGS2 expression is induced by cytokines and growth factors and is particularly increased during inflammation.^{25,26} PTGS2 has also been revealed to be expressed in many solid tumor types such as human gastric carcinoma,²⁷ pancreatic adenocarcinomas,²⁸ and prostate adenocarcinoma²⁹ and acts on a series of cell signaling pathways involving cell proliferation, angiogenesis, apoptosis, invasion, and immunosuppression, thereby increasing tumor progression. Here, PTGS2 serves as a tumor promoter in MM with high protein and mRNA levels. Similarly, it is indicated that the knockdown of PTGS2 leads to the inhibition of cell proliferation, migration, and colony formation and is accompanied by the promotion of cell apoptosis. Knockdown of PTGS2 also significantly attenuates the regulatory roles of overexpressed EIF3B on MM cells, including the inhibition of cell proliferation, migration, and colony formation as well as the promotion of apoptosis.

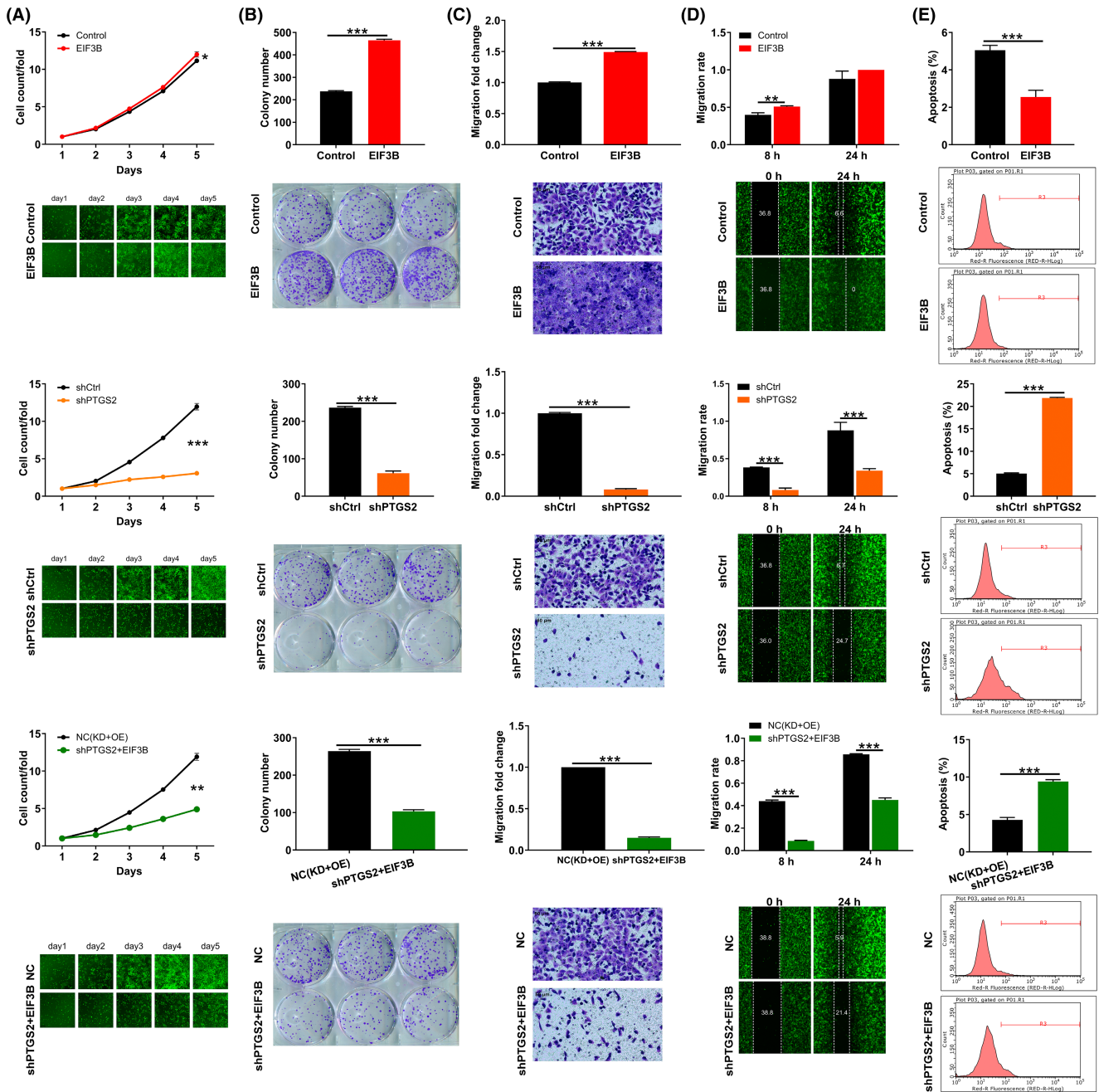


FIGURE 5 The promotion effects of EIF3B overexpression on melanoma progression was reversed by downregulating PTGS2. A, Celigo cell-counting assay was employed to show the effects of EIF3B, shPTGS2, and EIF3B+shPTGS2 lentiviruses on A375 cell proliferation. B, Colony formation assay was used to evaluate the abilities of A375 cells to form colonies after transfecting EIF3B, shPTGS2, and EIF3B+shPTGS2 lentiviruses. C, D, The migration rate of A375 cells was detected in the EIF3B, shPTGS2, and EIF3B+shPTGS2 groups by transwell assay (C) and wound-healing assay (D). Magnification: 200 \times . E, Flow cytometry was performed to show the effects of EIF3B, shPTGS2, and EIF3B+shPTGS2 lentiviruses on A375 cell apoptosis. All the experiments were performed in triplicate. The data are expressed as mean \pm SD. ** $p < 0.01$, *** $p < 0.001$

Furthermore, we found that the proliferation and migration inhibited by silencing of EIF3B were partially recovered by overexpression of PTGS2. Therefore, we believe that the mediator of EIF3B regulating melanoma is not only PTGS2—other targets or molecular signaling pathways may also be involved. Published literature reported that high PTGS2 expression in tumor-associated macrophages (TAMs) promotes endocrine resistance by the PI3K/Akt/mTOR pathway.³⁰

Another study on prostatic carcinoma revealed that PTGS2 could activate the AKT/NF- κ B pathway through phosphorylation.³¹ Moreover, Gan et al. demonstrated that PTGS2 in TAMs promotes metastatic potential of breast cancer cells through the Akt pathway.³² From this, we inferred that in melanoma, PTGS2 might mediate the wide cellular functions of EIF3B through the AKT signal pathway, which requires in-depth research in the future.

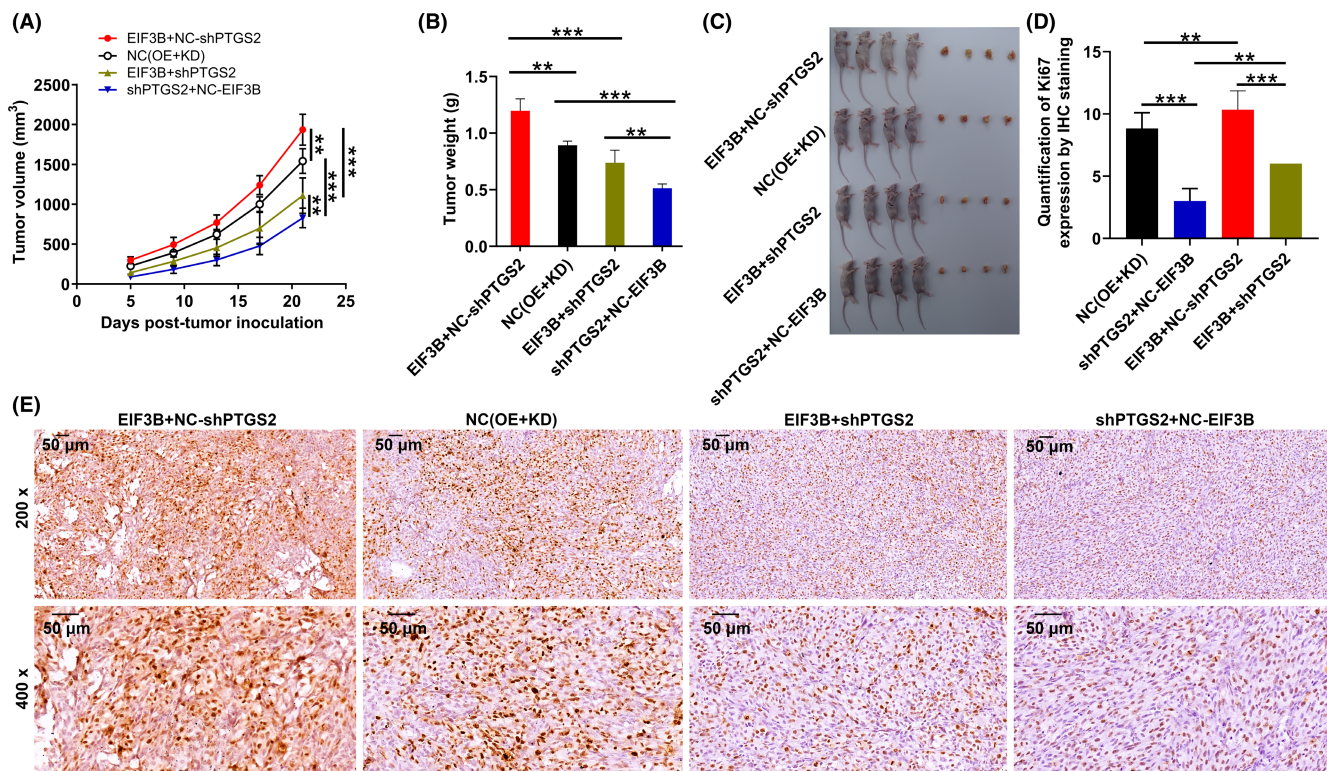


FIGURE 6 The effects of the EIF3B-PTGS2 axis in malignant melanoma tumor growth. A, B, The volume (A) and weight (B) of tumors from mice of the NC, EIF3B, shPTGS2, and EIF3B + shPTGS2 groups were checked from feeding to sacrifice. C, After sacrificing mice, the obtained tumors were weighed and photographed. D, E, The value of Ki-67 was detected by IHC analysis in tumor sections from mice of the NC, EIF3B, shPTGS2, and EIF3B + shPTGS2 groups. Magnification: 200 \times , 400 \times . Results are presented as mean \pm SD. *** p < 0.001

In summary, our current work demonstrated that EIF3B exerts a tumor-promoting role in MM by targeting PTGS2. EIF3B may represent a promising candidate target for the treatment of MM.

AUTHOR CONTRIBUTIONS

Pengli Fang, Yikai Han, Wang Ma and Guangshuai Li designed this research. Yanhong Qu, Xin Wang and Yong Zhang operated the cell and animal experiments. Pengli Fang, Wei Zhang and Na Zhang conducted the data procession and analysis. Pengli Fang completed the manuscript which was reviewed by Wang Ma and Guangshuai Li. All the authors have confirmed the submission of this manuscript.

ACKNOWLEDGMENTS

None.

FUNDING INFORMATION

This study was conducted with support from the Henan Physical Medicine Society Foundation (No. 2021HYTP058).

DISCLOSURE

The authors declare that they have no conflict of interest.

ETHICAL APPROVAL

Approval of the research protocol by an Institutional Reviewer Board: Laboratory Animal Center of Zhengzhou University.

Informed Consent: All the patients signed informed consent before collecting samples.

Registry and the Registration No. of the study: No. ZZU-LAC20200911 (18).

Animal Studies: All animal experiments were approved by the Laboratory Animal Center of Zhengzhou University [No. ZZU-LAC20200911 (18)].

ORCID

Wang Ma <https://orcid.org/0000-0003-0517-7115>

REFERENCES

- Clark WH Jr, Elder DE, Van Horn M. The biologic forms of malignant melanoma. *Hum Pathol*. 1986;17:443-450.
- Freedman DM, Dosemeci M, McGlynn K. Sunlight and mortality from breast, ovarian, colon, prostate, and non-melanoma skin cancer: a composite death certificate based case-control study. *Occup Environ Med*. 2002;59:257-262.
- Balch CM, Gershenwald JE, Soong SJ, et al. Final version of 2009 AJCC melanoma staging and classification. *J Clin Oncol*. 2009;27:6199-6206.
- Singh AD, Turell ME, Topham AK. Uveal melanoma: trends in incidence, treatment, and survival. *Ophthalmology*. 2011;118:1881-1885.
- Dhomen N, Marais R. BRAF signaling and targeted therapies in melanoma. *Hematol Oncol Clin North Am*. 2009;23:529-545. ix.
- Guo J, Si L, Kong Y, et al. Phase II, open-label, single-arm trial of imatinib mesylate in patients with metastatic melanoma harboring c-kit mutation or amplification. *J Clin Oncol*. 2011;29:2904-2909.

7. Brose MS, Volpe P, Feldman M, et al. BRAF and RAS mutations in human lung cancer and melanoma. *Cancer Res.* 2002;62:6997-7000.
8. Spriggs KA, Bushell M, Willis AE. Translational regulation of gene expression during conditions of cell stress. *Mol Cell.* 2010;40:228-237.
9. Jackson RJ, Hellen CU, Pestova TV. The mechanism of eukaryotic translation initiation and principles of its regulation. *Nat Rev Mol Cell Biol.* 2010;11:113-127.
10. des Georges A, Dhote V, Kuhn L, et al. Structure of mammalian eIF3 in the context of the 43S preinitiation complex. *Nature.* 2015;525:491-495.
11. Block KL, Vornlocher HP, Hershey JW. Characterization of cDNAs encoding the p44 and p35 subunits of human translation initiation factor eIF3. *J Biol Chem.* 1998;273:31901-31908.
12. Zang Y, Zhang X, Yan L, et al. Eukaryotic translation initiation factor 3b is both a promising prognostic biomarker and a potential therapeutic target for patients with clear cell renal cell carcinoma. *J Cancer.* 2017;8:3049-3061.
13. Xu F, Xu CZ, Gu J, et al. Eukaryotic translation initiation factor 3B accelerates the progression of esophageal squamous cell carcinoma by activating β -catenin signaling pathway. *Oncotarget.* 2016;7:43401-43411.
14. Wang L, Wen X, Luan F, et al. EIF3B is associated with poor outcomes in gastric cancer patients and promotes cancer progression via the PI3K/AKT/mTOR signaling pathway. *Cancer Manag Res.* 2019;11:7877-7891.
15. Wang H, Ru Y, Sanchez-Carbayo M, Wang X, Kieft JS, Theodorescu D. Translation initiation factor eIF3b expression in human cancer and its role in tumor growth and lung colonization. *Clin Cancer Res.* 2013;19:2850-2860.
16. Wang R, Wang G. Protein modification and autophagy activation. *Adv Exp Med Biol.* 2019;1206:237-259.
17. Inobe T, Matouschek A. Paradigms of protein degradation by the proteasome. *Curr Opin Struct Biol.* 2014;24:156-164.
18. Kang DC, Gao XQ, Ge QF, Zhou GH, Zhang WG. Effects of ultrasound on the beef structure and water distribution during curing through protein degradation and modification. *Ultrason Sonochem.* 2017;38:317-325.
19. Balch CM, Buzaid AC, Soong SJ, et al. Final version of the American joint committee on cancer staging system for cutaneous melanoma. *J Clin Oncol.* 2001;19:3635-3648.
20. Liang H, Ding X, Zhou C, et al. Knockdown of eukaryotic translation initiation factors 3B (EIF3B) inhibits proliferation and promotes apoptosis in glioblastoma cells. *Neurol Sci.* 2012;33:1057-1062.
21. Xiang P, Sun Y, Fang Z, Yan K, Fan Y. Eukaryotic translation initiation factor 3 subunit b is a novel oncogenic factor in prostate cancer. *Mamm Genome.* 2020;31:197-204.
22. Nandi D, Tahiliani P, Kumar A, Chandu D. The ubiquitin-proteasome system. *J Biosci.* 2006;31:137-155.
23. Qi J, Ronai ZA. Dysregulation of ubiquitin ligases in cancer. *Drug Resist Updat.* 2015;23:1-11.
24. Zheng Q, Huang T, Zhang L, et al. Dysregulation of ubiquitin-proteasome system in neurodegenerative diseases. *Front Aging Neurosci.* 2016;8:303.
25. DeWitt DL, Meade EA. Serum and glucocorticoid regulation of gene transcription and expression of the prostaglandin H synthase-1 and prostaglandin H synthase-2 isozymes. *Arch Biochem Biophys.* 1993;306:94-102.
26. Hamasaki Y, Kitzler J, Hardman R, Nettesheim P, Eling TE. Phorbol ester and epidermal growth factor enhance the expression of two inducible prostaglandin H synthase genes in rat tracheal epithelial cells. *Arch Biochem Biophys.* 1993;304:226-234.
27. Ristimäki A, Honkanen N, Jänkälä H, Sipponen P, Härkönen M. Expression of cyclooxygenase-2 in human gastric carcinoma. *Cancer Res.* 1997;57:1276-1280.
28. Yip-Schneider MT, Barnard DS, Billings SD, et al. Cyclooxygenase-2 expression in human pancreatic adenocarcinomas. *Carcinogenesis.* 2000;21:139-146.
29. Lee LM, Pan CC, Cheng CJ, Chi CW, Liu TY. Expression of cyclooxygenase-2 in prostate adenocarcinoma and benign prostatic hyperplasia. *Anticancer Res.* 2001;21:1291-1294.
30. Qin Q, Ji H, Li D, Zhang H, Zhang Z, Zhang Q. Tumor-associated macrophages increase COX-2 expression promoting endocrine resistance in breast cancer via the PI3K/Akt/mTOR pathway. *Neoplasma.* 2021;68:938-946.
31. Zhang Z. MiR-124-3p suppresses prostatic carcinoma by targeting PTGS2 through the AKT/NF-kappaB pathway. *Mol Biotechnol.* 2021;63:621-630.
32. Gan L, Qiu Z, Huang J, et al. Cyclooxygenase-2 in tumor-associated macrophages promotes metastatic potential of breast cancer cells through Akt pathway. *Int J Biol Sci.* 2016;12:1533-1543.

SUPPORTING INFORMATION

Additional supporting information can be found online in the Supporting Information section at the end of this article.

How to cite this article: Fang P, Han Y, Qu Y, et al. EIF3B stabilizes PTGS2 expression by counteracting MDM2-mediated ubiquitination to promote the development and progression of malignant melanoma. *Cancer Sci.* 2022;113:4181-4192. doi: [10.1111/cas.15543](https://doi.org/10.1111/cas.15543)